SPATIAL RESOLUTION ESTIMATION OF CBERS-1 AND CBERS-2 CCD CAMERA

K. BENSEBAA*, G. J. F. BANON, L. M. G. FONSECA

Image Processing Division - National Institute for Space Research (INPE)
Av. dos Astronautas, 1758, 12201-027 São José dos Campos, Brazil

The first China-Brazil Earth Resources Satellite (CBERS-1) was launched in 1999 and was substituted in 2003 by CBERS-2. CBERS- 1 and CBERS-2 have the same specifications and carry three sensors: Wide Field Imager (WFI), High Resolution CCD Camera (CCD) and Infrared Multispectral Scanner (IRMSS). In general, the images may have a blurred appearance due to the cumulative effects of the sensor instruments and image motion produced by the satellite movement. This blurring effect can be described by the Point Spread Function (PSF) which enables an objective assessment of spatial resolution through the parameter known as EIFOV (Effective Instantaneous Field of View). Therefore, this work describes three approaches to estimate the effective spatial resolution of CBERS-CCD cameras. The first approach uses artificial target to estimate the EIFOV in across-track and along-track directions simultaneously, while the other approaches use natural targets to estimate the EIFOV in both directions separately.

Keywords: CCD Camera, Spatial Resolution, Estimation, Simulation, Targets.

1. Introduction

In the last two decades China and Brazil have jointly developed CBERS satellites (China-Brazil Earth Resources Satellite). CBERS-1 and CBERS-2 satellites were launched on October 14, 1999 and on October 21, 2003, respectively, by the Chinese launcher Long-March 4B, from the Tayuan Launch Center, in the Popular Republic of China. They carry three instruments: CCD (Charge Coupled Device) camera, IRMSS (Infrared MSS) and WFI (Wide Field Imager), which capture optical images of the Earth surface and transmit them to ground stations.

After launching, the imaging system performance usually changes due to its exposition to the space environment. Besides, the cumulative effects of the optical and electronic systems (diffraction, aberrations, focusing error, oversampling) and the image motion induced by the movement of the satellite degrade the camera spatial resolution (Leger et al. 2002). Hence, the images may have a blurred appearance that is likely to compromise their visual quality and analysis tasks.

One way to evaluate the blurring effect of a sensor is through its effective spatial resolution which can be determined in terms of the Point Spread Function (PSF) or Modulation Transfer Function (MTF) of the sensor. The MTF (or PSF) of an imaging system is of fundamental importance in both the initial specification and design of the system and in subsequent detailed analysis of the images it produces.

Another important parameter is the Effective Instantaneous Field of View (EIFOV), which is used to measure the system performance and it is defined as a function of the sensor. Moreover, the EIFOV parameter enables a comparison among different sensors with similar nominal spatial resolution. In general the PSF can be approximated by a Gaussian function (Luxen and Forster, 2002). When the PSF is

approximated by a Gaussian function with standard deviation σ, the EIFOV is 2.66σ (Slater, 1980; Banon and Santos, 1993).

Basically, there are three approaches to determine the PSF or MTF of an imaging system. They are based on experimental methods or on theoretical modelling of the physical processes in study. The first one uses artificial or natural targets with well-defined shape and size as airport runways, bridges, edges, etc. Storey (2001) has provided a methodology for on-orbit spatial resolution estimation of Landsat-7 ETM + sensor by using a Causeway bridge image (Louisiana – USA). Choi and Helder (2003) have used an airport runway and a tarp placed on the ground for on-orbit MTF measurement of IKONOS satellite sensor. Other works (Nelson e Barry, 2001; Leger et al., 2002; Luxen e Forstner, 2002) have also used similar approaches to estimate the system PSF. The second approach consists of adjusting a simulated low resolution image to an image acquired by the sensor under study. According to Storey (2001), this method works satisfactorily if the two sets of imagery are acquired at or near the same time or, at least, under similar conditions to avoid the problems associated with temporal variations. The third approach uses the image system specifications to model its spatial response. Fonseca and Mascarenhas (1987) and Markham (1985) have used this methodology to determine the spatial response of the TM sensor (Landsat satellite).

In order to evaluate the spatial response of CBERS-CCD cameras, this work presents three experiments based on the approaches mentioned before. The first one uses an image of a black squared target simulated in the Gobi desert (China). The CCD spatial response is modelled as 2D Gaussian function which is characterized by two parameters: one in along-track direction and the other one in across-track direction. The EIFOV values are then derived from these parameters (Bensebaa et al., 2004a). The second experiment models the imaging system point spread function by a separable Gaussian function in the across- and along-track directions. Images of natural targets such as the Rio-Niteroi Bridge over Guanabara Bay (Brasil) and Causeway bridge over the Lake Pontchartrain (United States) are used to estimate the spatial resolution in the along- and across-track directions, respectively (Bensebaa et al., 2004b). The third experiment determines the spatial resolution of the CBERS-CCD cameras using a higher spatial resolution image acquired by the SPOT-4 satellite and an image of the same scene acquired by CBERS satellite (Bensebaa et al., 2004c).

This paper is organized in the following way. Section 2 gives a brief overview of CBERS-CCD camera. Section 3 describes the first approach to estimate on-orbit CBERS CCD spatial resolution using images of an artificial black squared target in the Gobi desert (China). Section 4 introduces a second approach using two natural targets: an image of the Rio-Niterói bridge, over Guanabara bay (Rio de Janeiro - Brazil), and an image of the Causeway bridge over Pontchartrain lake (Louisiana - USA). Section 5 presents the last approach that uses an image of higher spatial resolution (SPOT-4) than that of a CBERS-CCD image. Finally, Section 6 presents the conclusions.

2. CBERS CCD camera

CBERS-1 and CBERS-2 CCD cameras have 4 spectral bands from visible to near infrared spectrum and one panchromatic band (Table. 1). It acquires the earth ground scenes by pushbroom scanning, on 778 km sun-synchronous orbit and provides images of 113 km wide strips with sampling rate of 20 meters at nadir. Since this camera has a sideways pointing capability of ± 32 degrees, it is capable of capturing stereoscopic images of a certain region.

The signal acquisition system operates in two channels called CCD1 and CCD2. The first one generates images corresponding to bands B2, B3 and B4 while the second generates images corresponding to bands B1, B3 and B5. In each channel (channel C1 and channel C2), three CCD arrays per band are combined to generate about 6000 pixels per row. A complete coverage cycle of the CCD camera takes 26 days.

Table 1. Spectral bands of the CCD sensor.

Spectral Bands	Band Number	Wavelength (μm)
Blue	1	0,45 - 0,52
Green	2	0,52 - 0,59
Red	3	0,63 - 0,69
Near-Infrared	4	0,77 - 0,89
Pan.	5	0,51 - 0,73

3. Spatial resolution estimation using an artificial target

The first experiment uses an artificial target simulated on the ground in the Gobi desert (China). The PSF is modeled as 2D Gaussian function that is characterized by two parameters corresponding to along- and across-track directions. The target image simulation is performed from the target model in order to find the optimal parameters that characterize the CCD camera PSF. Details about the modeling of the PSF, target image, and simulated target are given in the next sections.

3.1 *Simulated Target*

The target is a dark squared tarp placed in the Gobi desert. The test local is situated at about 35 km west of Dunhuang city in Gansu Province, China. Its location is about 30 km from south to north and 40 km from east to west. The size of the black target is 60 meters x 60 meters, which corresponds to a sub-image of 3x3 pixels. Besides, the black target edge is aligned to the along track direction of the satellite (Fig. 3.1).

Figure 3.1. Setting up the black tarp in the Gobi desert.

The target images used in this experiment were acquired by CBERS-1 on September 4, 2000 and by CBERS-2 on August 19, 2004. Fig. 3.2 shows the black target in the center of the image (CBERS-1, band 3). In order to facilitate the visualization, the image was zoomed up. In this experiment, only Bands B2, B3, and B4 were processed.

The raw CBERS-1 images (without calibration) present a striping effect: odd columns are brighter than even columns (Fig. 3.2). The images are processed in order to remove the stripping effect by adjusting the mean and standard deviation of the odd and even columns as described in Banon (2000).

Let E be the image domain with an even number of columns. Let E_e and E_o be the sets of pixel positions belonging, respectively, to the even and odd columns of E. Let f be the original CBERS-1 image. The calibrated image g is given by:

$$g(x) = \begin{cases} a_e f(x) + b_e & \text{if } x \in E_e \\ a_o f(x) + b_o & \text{if } x \in E_o \end{cases}, \quad x \in E,$$

where

$$a_e = \frac{s}{s_e},\ a_o = \frac{s}{s_o},\ b_e = m - a_e.m_e,\ b_o = m - a_o.m_o$$

and m_e and m_o are the mean values of the original image restricted to E_e and E_o, respectively. s_e and s_o are the standard deviations of the original image restricted to E_e and E_o, respectively, and $m = (m_e + m_o)/2$ and $s = (s_e + s_o)/2$. After the processing, one can observe (Fig. 3.3) that the striping effect has been completely eliminated without removing the target information.

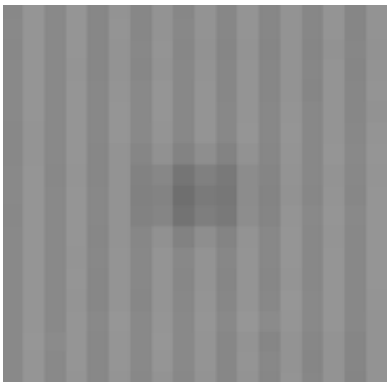

Figure 3.2. Original target image (band 3).

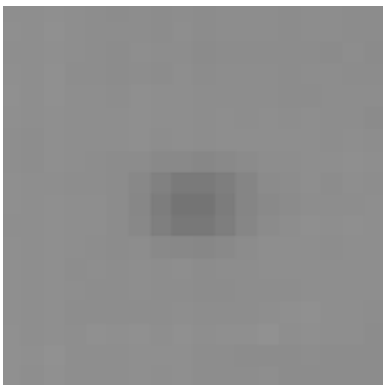

Figure 3.3: Target image after destriping (band 3).

3.2 *Digital target model*

Let Z be the set of integer numbers and let $\mathbf{Z^2}$ be the Cartesian product of Z by itself. Let $x \in Z$, we denote by $\underline{x}$ the pair (x, x) of $\mathbf{Z^2}$. For example $\underline{10}$ stands for the pair (10,10). Let F be a finite square of Z^2 with an odd number of lines and columns representing the digital scene domain in which the distance between two consecutive horizontal or vertical points is one meter, for convenience. Let u be the center point of F. Based on radiometric and geometric features of the target, the digital target model is the function f on F, for every $x \in F$, given by:

$$f_t(x) = \begin{cases} t & \text{if } x \in [u - \underline{30}, u + \underline{30}]. \\ s & \text{otherwise.} \end{cases}$$

where s and t are the background (desert) and target radiometry values, respectively. [a, b] is the rectangle of $\mathbf{Z^2}$ having a as lower left corner and b as upper right corner. One observes that the digital target model is centered at u and the target size is 60m × 60m (Fig. 3.4).

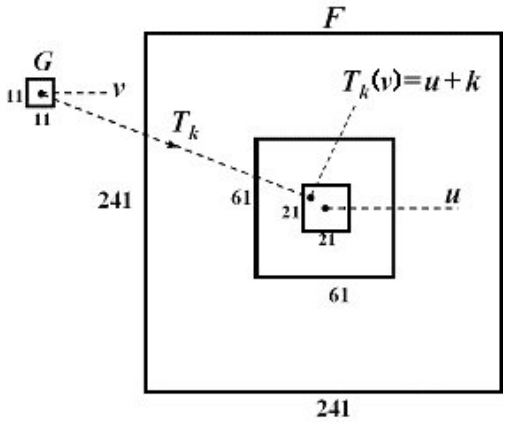

Figure 3.4: Digital target model.

3.3 *Target image simulation*

Let G be a finite square of $\mathbf{Z}^2$ with an odd number of rows and columns, representing the target image domain. Let v be the center point of G and let T_k be a geometric transformation from G to F given by:

$$T_k(y) = 20.(y - v) + u + k,$$

for every y ∈ G and k ∈ $\mathbf{Z}^2$.

The transformation T_k is the system geometric model, where the value 20 represents the distance (in meters) between two consecutive horizontal or vertical pixel positions (sampling rate). The offset k defines how far the transformation of the target image domain center v is from the digital scene domain center u (Fig. 3.4). By assuming that the imaging system is linear, the simulated target image is

$$(f_t * h_{\sigma_1,\sigma_2}) \circ T_k$$

where h is the sensor PSF , * is the (circular) convolution product (u is being chosen as the origin) on F, and ∘ is the mapping composition. By composition definition, one can observe that the simulated target image is a function on G.

3.4 *PSF identification*

The CBERS CCD point spread function is modeled as a separable 2D Gaussian function h_{σ_1,σ_2} on F, with center at $u(u_1,u_2)$, that is, for every $(x_1, x_2) \in F$,

$$h_{\sigma_1,\sigma_2}(x_1,x_2) = \frac{1}{2\pi\sigma_1\sigma_2} e^{-\left(\frac{(x_1-u_1)^2}{2\sigma_1^2} + \frac{(x_2-u_2)^2}{2\sigma_2^2}\right)},$$

where σ_1 and σ_2 are the standard deviation of the Gaussian model.

Let the root mean square error, RMS (f_t, g), be the real number given by

$$\mathrm{RMS}(f_t, g) = \left(\sum_{y \in G} \left((f_t * h_{\sigma_1,\sigma_2})(T_k(y)) - g(y) \right)^2 \right)^{1/2} .$$

Let g be the target image defined on G, such that $g(v)$ has the lowest (recall that the target is black) value among all the pixel values of g. The PSF identification consists of finding σ_1 and σ_2 such that g and $(f_t * h_{\sigma_1,\sigma_2}) \circ T_k$ best fits under the root mean square criteria.

The PSF identification is a two-step procedure. In the first step, $t = g(v)$ and one looks for k, σ_1 and σ_2, which minimizes RMS(f_t, g). Because $g(v)$ is the lowest value among the pixel values of g, the domain of k reduces to [-10, 10] of $\mathbf{Z}^2$.

In the second step, one uses the previous optimum $k = (k_1, k_2)$ and one looks for t, σ_1 and σ_2 which minimizes RMS (f_t, g). The block diagram shown in the Fig. 3.5 illustrates the PSF identification procedure. The desert radiometry s was estimated by averaging the pixel values in the target neighborhood.

In the above procedure, we have used F = [1, 241], u = 121, G = [1, 11], v = 6. The target radiometry value t was considered within the following interval of $\mathbf{Z}$:

$$[g(v) - 2, g(v) + 2]$$

Finally, the optimal values of σ_1 and σ_2 were obtained by nonlinear programming (Himmelblau, 1972).

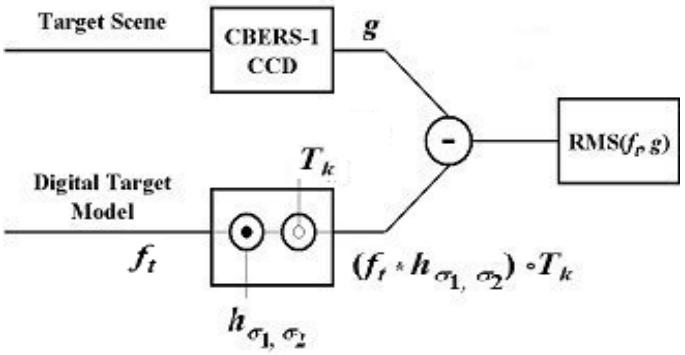

Figure 3.5: Block diagram of the PSF identification process.

3.5 *Results*

Tables 3.1 and 3.2 show the spatial resolution values before the launching of CBERS-1 and CBERS-2 respectively. One can observe that the EIFOV values of band 4 are higher than those of bands 2 and 3. This blurring effect in band 4 of CBERS-1 CCD camera was observed before launching and it is due to a problem in the camera assembly. Tables 3.3 and 3.4 show the optimal EIFOV values, respectively for CBERS-1 and CBERS-2, in the along- and across-track directions. Figure 3.6 and Figure 3.7 show the along- and across-track fitting between original data and simulated data for band 3.

Table 3.1: Pre-launching spatial resolution estimation (CBERS-1). (SOURCE: Fonseca et al., 2002).

Bands	EIFOVs(m)
B_2	33.1
B_3	35.3
B_4	68.2

Table 3.2: Pre-launching spatial resolution estimation (CBERS-2). (SOURCE: Fonseca et al., 2004).

Bands	EIFOVs(m)
B_2	31.0
B_3	31.0
B_4	53.0

Table 3.3: Estimated parameters for CBERS-1.

Bands	EIFOV (m) along-track direction	EIFOV (m) across-track direction
B2	34	68
B3	32	68
B4	51	76

Table 3.4 Estimated parameters for CBERS-2.

Bands	EIFOV (m) along-track direction	EIFOV (m) across-track direction
B2	32	56
B3	43	54
B4	31	66

One can observe that spatial resolution was degraded for all bands in the across-track direction for both cameras CBERS-1 CCD and CBERS-2 CCD. As expected, the degradation was observed in band 4 of CBERS-1 CCD camera. On the order hand, band 3 of CBERS-1 CCD was also degraded after launching.

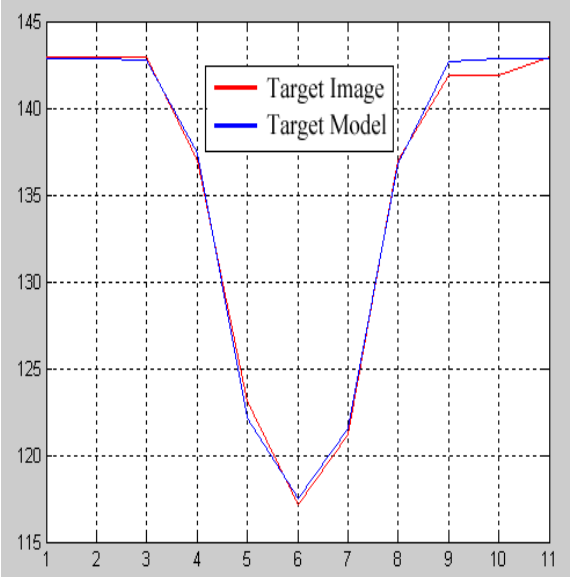

Figure 3.6: Along-track fitting for band 3 of CBERS-1.

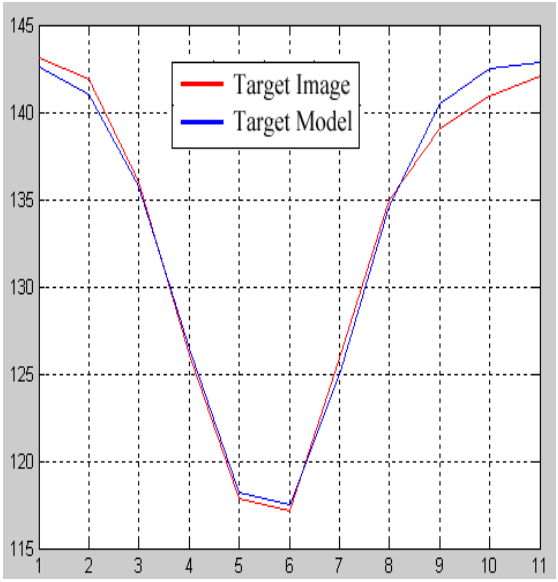

Figure 3.7: Along-track fitting for band 3 of CBERS-1

4. Natural target

This experiment uses bridges as targets. Two bridges are used to estimate the PSF in both directions: along- and across-track. The PSF identification is accomplished in three steps: (1) bridges modelling, (2) bridge axis identification and (3) bridge image simulation from the bridge model. These steps are described in the following sections.

4.1 *Target Images*

The Rio-Niterói bridge over Guanabara Bay (Figure 4.1 and Figure 4.2) was chosen as target to estimate the spatial resolution in the along-track direction. This bridge is 13.29-km long with only one deck and its width is 26.6 meters. In order to estimate the spatial resolution in across-track direction, the Causeway bridge over the Pontchartrain lake (Figure 4.3 and Figure 4.4) was used. This bridge is constituted of two

decks and a gap between them. It is 38.62-km long where each deck is 10.0 meters wide and the gap is 24.4 meters wide. The two decks were constructed at different times (1956 and 1969) and exhibit slightly different reflectance values. In addition, the water background is reasonably uniform.

The Rio-Niterói bridge images were acquired by CBERS-1 on December 02, 2001 and by CBERS-2 on July 10, 2004. The Lake Pontchartrain Causeway bridge images were acquired by CBERS-1 on October 06, 2002 and by CBERS-2 on September 25, 2004.

The red rectangles (Figure 4.5 and 4.6) show the sub-images selected for the experiment. Figures 4.7a and 4.8a show the original Rio-Niterói bridge and Causeway bridge images (band 3), respectively. As the images are not calibrated, they present a striping effect. Using the algorithm described in the section 3.2, the images were processed. Figures 4.7b and 4.8b show the bridge images after being processed. In order to facilitate the visualization, the images were enhanced and zoomed up.

Fig.4.1 Map of the Rio-Niterói bridge over the Guanabara bay.

Fig.4.2 Map of the Causeway bridge over the Pontchartrain lake.

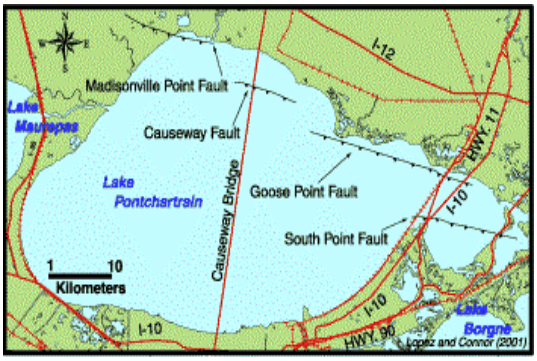

Fig.4.3 Aerial image of the Rio-Niterói bridge over the Guanabara bay.

Fig.4.4 Aerial image of the Causeway bridge over the Pontchartrain lake.

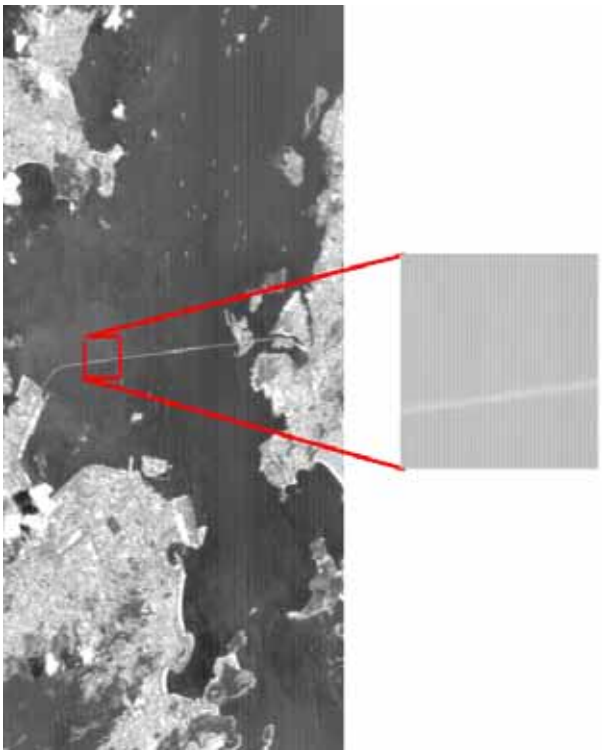

4.5 Selected sub-image of Rio-Niteroi bridge.

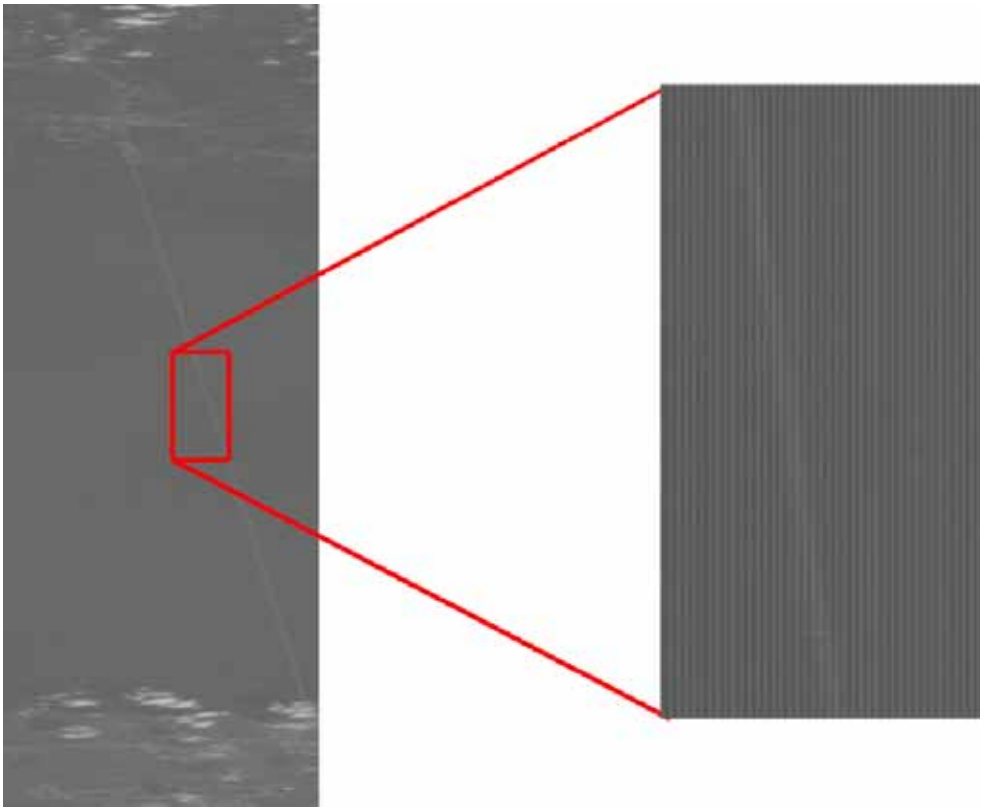

4.6 Selected sub-image of Causeway bridge.

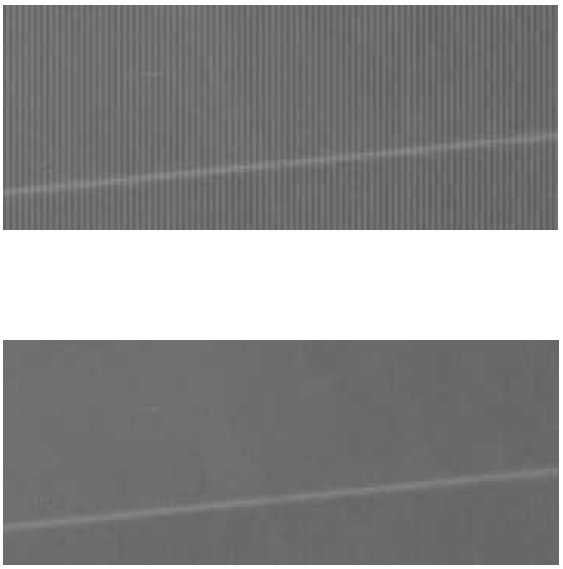

Fig.4.7 Original and processed Rio- Niterói bridge image (band 3) .

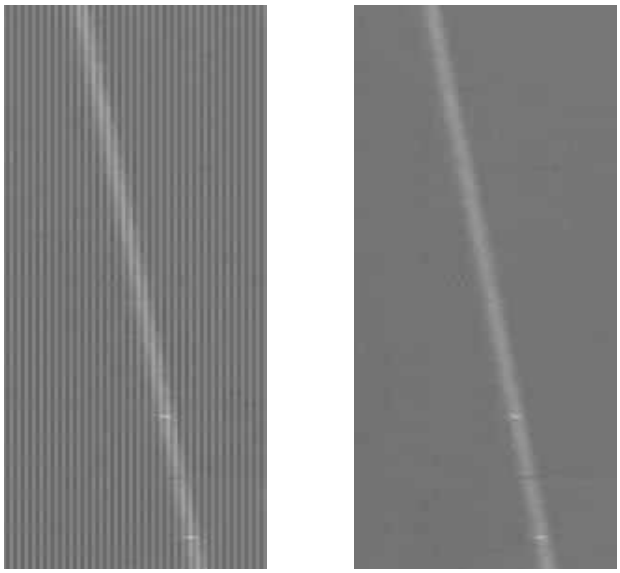

Fig.4.8 Original and processed Causeway bridge image (band3).

4.2 *Digital bridge model*

Rio-Niterói bridge

Let **Z** be the set of integer numbers. Let F_1 be a finite interval of **Z** with an odd number of elements, which represents a vertical line of the digital scene domain. The distance between two consecutive elements is one meter, for convenience.

Let u_1 be the "center" point of F_1. Based on its radiometric and geometric features, the bridge over the Guanabara bay, is modeled as the function f_1 on F_1 given by

$$f_1(x) = \begin{cases} t & \text{if } x \in [u_1 - 13, u_1 + 13] \\ s & \text{otherwise} \end{cases} \qquad x \in F_1 \text{ ,}$$

where s, t are the background (water body) and the deck radiometry, respectively.

Causeway bridge

Let F_2 be a finite interval of **Z** with an even number of elements representing an horizontal line of the digital scene domain. For convenience, the distance between two consecutive elements is one meter. Let u_2 be the center point of F_2. Based on its radiometric and geometric features, the bridge over the Pontchartrain lake, is modeled as the function f_2 on F_2 given by

$$f_2(x) = \begin{cases} t_1 & \text{if } x \in [u_2 - 22, u_2 - 13] \\ t_2 & \text{if } x \in [u_2 + 13, u_2 + 22] \\ s & \text{otherwise} \end{cases} \qquad x \in F_2 \text{ ,}$$

where s, t_1, t_2 are the background, left deck and right deck radiometry values, respectively.

4.3 *Bridge axis identification*

According to Figures 4.7 and 4.8, the bridge axis is a straight line. Consequently, it can be represented by a linear model. Let the bridge image g be a mapping from $G = \mathbf{m} \times \mathbf{n}$, its domain, to K, its gray–scale, where $\mathbf{m} = [1, m] \subset \mathbf{Z}$ and $\mathbf{n} = [1, n] \subset \mathbf{Z}$. m and n are the number of rows and columns of the image *g*, respectively.

Rio-Niterói bridge

Let c_1 be the mapping from **n** to **m** such that $c_1(j)$ ($j \in \mathbf{n}$) is the row number in **m**, for which $g(c_1(j), j)$ is maximum in $\{g(i,j)\}_{i \in \mathbf{m}}$

Let $a, b \in \mathbf{R}$, such that

$$\sum_{i \in \mathbf{m}} ((a.j + b) - c_1(j))^2 \text{ is minimum,}$$

then $a.j + b$ ($j \in \mathbf{n}$) is the bridge center estimation along column *j*.

Causeway bridge

Let c_2 be the mapping from **m** to **n** such that $c_2(i)$ ($i \in \mathbf{m}$) is the column number in **n**, for which $g(i, c_2(i))$ is maximum in $\{g(i,j)\}_{j \in \mathbf{n}}$

Let $a, b \in \mathbf{R}$, such that

$$\sum_{i \in \mathbf{m}} ((a.i + b) - c_2(i))^2 \text{ is minimum,}$$

then $a.i + b$ ($i \in \mathbf{m}$) is the bridge center estimation along row *i*. In both cases (Rio-Niterói and Causeway bridge), there are more measurements available than unknown parameters (*a* and *b*). Therefore, the QR-decomposition was used to generate a least square solution of an over-determined system of linear equations (Kreyszig, 1993).

4.4 *Bridge image simulation*

Rio-Niterói bridge

The procedures for the bridge image simulation are based on the estimation of bridge center described in the Section 4.3.

For a given column $j \in \mathbf{n}$, let $\hat{c}_1 = a.j + b$. Let G_1, be a finite interval of **Z** with an odd number of elements, denoted by *p*. Let $v = (p + 1) / 2$ be the center of G_1. Let us assume that $G_1 + \left\lfloor \hat{c}_1 + \frac{1}{2} \right\rfloor - v \subset \mathbf{m}$, ($\lfloor x \rfloor$ is the inter part of *x*).

Let T_{k_1} be a geometric transformation from G_1 to F_1 given by

$$T_{k_1}(y) = \left\lfloor 20 . (y - v) + \frac{1}{2} \right\rfloor + u_1 + k_1 \qquad y \in G_1 \text{ ,}$$

where

$$k_1 = \left\lfloor 20 \left(\left\lfloor \hat{c}_1 + \frac{1}{2} \right\rfloor - \hat{c}_1 \right) + \frac{1}{2} \right\rfloor \quad .$$

In the above definition, u_1 is the center of the bridge, and k_1 represents how far the transformation of v is from u_1. Figure 4.9 shows the Rio-Niterói bridge model.

Causeway bridge

This simulation is similar to the one of Rio-Niterói bridge. For a given row $i \in \mathbf{m}$, let $\hat{c}_2 = a.i + b$. Let G_2, be a finite interval of **Z** with an even number of elements, denoted p. Let assume that $G_2 + \left\lfloor \hat{c}_2 \right\rfloor - \frac{p}{2} \subset \mathbf{n}$.

Let T_{k_2} be a geometric transformation from G_2 to F_2 given by

$$T_{k_2}(y) = 20.(y - v) + u_2 + k_2 \qquad y \in G_2 \ ,$$

where $v = (p + 1) / 2$ is the "center"of G_2, u_2 is the center of the bridge and k_2 represents how far the transformation of v is from u_2.

In the Causeway bridge image simulation, the bridge center estimation $\hat{c}_2$ is biased due to the different radiometry values of the two decks. Accordingly, k_2 is expressed as

$$k_2 = k_2' + \Delta$$

where

$$k_2' = \left\lfloor 20 \left(\frac{1}{2} + \left\lfloor \hat{c}_2 \right\rfloor - \hat{c}_2 \right) + \frac{1}{2} \right\rfloor$$

and Δ is a corrective term that takes into account the bridge center estimation bias. Since Δ assumes only a few integer values, its estimation can be based on an exhaustive search. Figure 4.10 shows the Causeway bridge model.

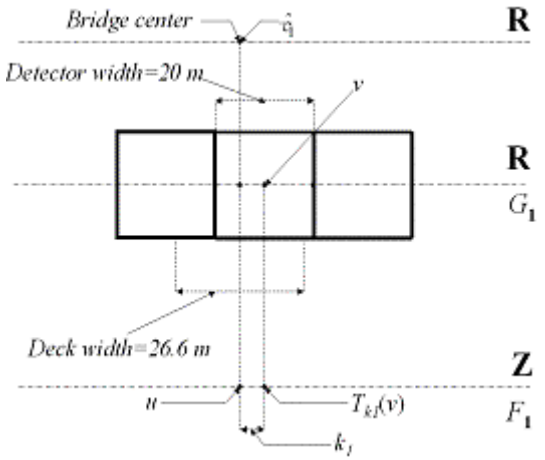

Fig.4.9 Rio-Niterói bridge model.

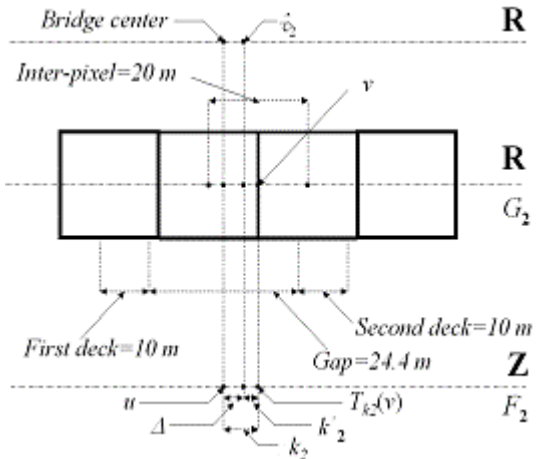

Fig.4.10 Causeway bridge model.

4.5 *PSF identification*

Similar to Section 3.4, the PSF is modeled as a 2D separable Gaussian function h_{σ_1,σ_2} on F_1 x F_2 centered at (u_1, u_2), that is,

$$h_{\sigma_1,\sigma_2}(x_1, x_2) = h_{\sigma_1}(x_1).h_{\sigma_2}(x_2) \ ,$$

where

$$h_{\sigma_1}(x_1) = \frac{1}{\sqrt{2\pi}\sigma_1} e^{-\frac{(x_1-u_1)^2}{2\sigma_1^2}} \qquad x_1 \in F_1$$

and

$$h_{\sigma_2}(x_2) = \frac{1}{\sqrt{2\pi}\sigma_2} e^{-\frac{(x_2-u_2)^2}{2\sigma_2^2}} \qquad x_2 \in F_2 \ .$$

Let g_1^j be the j^{th} bridge image column defined on G_1 given by

$$g_1^j(y) = g\left(\left\lfloor \hat{c}_1 + \frac{1}{2} \right\rfloor - v + y, j\right)$$

and let g_2^i be the i^{th} bridge image row defined on G_2 given by

$$g_2^i(y) = g\left(i, \left\lfloor \hat{c}_2 \right\rfloor - \frac{p}{2} + y\right) \ .$$

The PSF identification in the along-track direction consists of finding σ_1 such that g_1^j and $(f_1 * h_{\sigma_1}) \circ T_{k1}$ best fit under the root mean square criteria. In the same way, the PSF identification in the across-track direction consists of finding σ_2 such that g_2^i and $(f_2 * h_{\sigma_2}) \circ T_{k2}$ best fit under the root mean square criteria.

Let RMS_1 be the real number given by

$$RMS_1 = \left(\sum_{y \in G_1} \left(\left(f_1 * h_{\sigma_1} \right)\left(T_{k_1}(y) \right) - g_1^j(y) \right)^2 \right)^{1/2} \ .$$

The along-track estimation procedure is performed in two steps. Firstly, we look for t, s and σ_1 that minimize RMS_1. Afterwards, using their mean values over all columns obtained from the first step, one looks for σ_1 that minimizes RMS_1. Let RMS_2 be the real number given by

$$RMS_2 = \left(\sum_{y \in G_2} \left(\left(f_2 * h_{\sigma_2} \right)\left(T_{k_2}(y) \right) - g_2^i(y) \right)^2 \right)^{1/2} \ .$$

The across-track estimation procedure is also performed in two steps. First of all, one looks for Δ, t_1, t_2, s and σ_2 that minimize RMS_2. Secondly, using their mean values over all rows obtained from the first step, we look for σ_2 that minimizes RMS_2.

For both simulations (in the along-track and across-track-directions) the optimum values of σ_1 and σ_2 have been obtained by nonlinear programming (Himmelblau, 1972).

4.6 *Results*

Tables 4.1 and 4.2 show the estimated EIFOV values of CBERS-1 and CBERS-2, respectively. The best fitting between the image and the simulated bridge image (band 3), in along- and across-track directions, are shown in Figure 4.11 and Figure 4.12, respectively. Four columns of the image are shown. The results are slightly different from those obtained by the first method. However, some differences are expected since the data used in the experiment were acquired at different times.

Table 4.1: Estimated EIFOV for CBERS-1.

Bands	EIFOV (m) along-track direction	EIFOV (m) across-track direction
B2	37	67
B3	40	67
B4	64	81

Table 4.2 Estimated EIFOV for CBERS-2.

Bands	EIFOV (m) along-track direction	EIFOV (m) across-track direction
B2	39	62
B3	47	62
B4	45	61

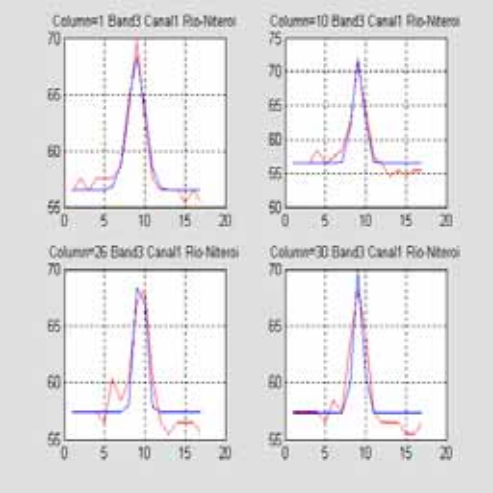

Figure 4.11 Along-track fitting (band 3).

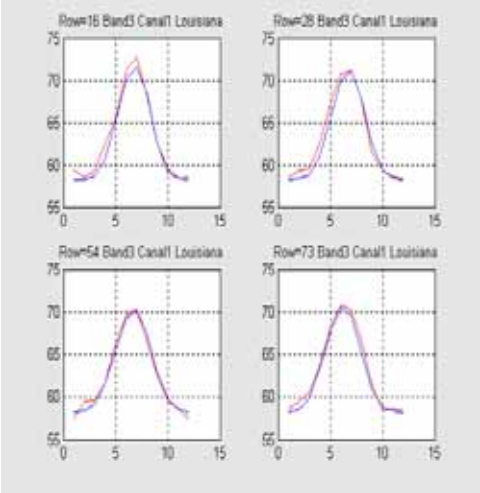

Figure 4.12 Across-track fitting (band 3).

5. Spatial resolution estimation using higher resolution images

The third experiment uses two images: a CBERS CCD image and an image of the same scene of higher resolution acquired by the SPOT-4 satellite. The method is iterative and the goal is to find a parameter of a low-pass filter that minimizes the Root Mean Square (RMS) difference between the CBERS and the filtered SPOT-4 images. Initially, the target images are selected and pre-processed to remove the stripping

effect. Then, the two images (CBERS and SPOT-4) are registered so that the same objects on the ground appear in the same position on the registered images.

5.1 *Target selection and data preparation*

In this case, the same CBERS-1 and CBERS-2 images used in Section 4 were selected. CBERS-1 CCD images of Rio-Niterói and Causeway bridges are shown in Figures 5.1 and 5.3, respectively. SPOT-4 images acquired on November 28, 2001 (Rio-Niteroi bridge) and on November 25, 2002 (Causeway bridge) are illustrated in the Figures 5.2 and 5.4, respectively.
CBERS and SPOT images were registered using an automatic image registration system (Fedorov et al., 2002, 2006). SPOT-4 images were taken as reference images in the registration process. Figures 5.5 and 5.6 show the results after the registration process.

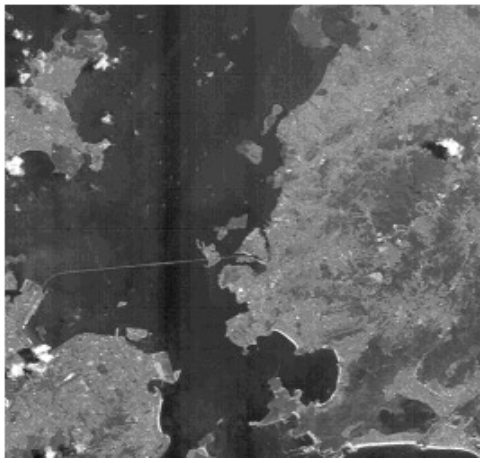

Fig.5.1 Rio-Niterói bridge image acquired by CBERS-1 (Band2).

Fig.5.2 Rio-Niterói bridge image acquired by SPOT 4 (Band2).

Fig.5.3 Causeweay bridge image acquired by CBERS-2 (Band2).

Fig.5.4 Causeweay bridge image acquired by SPOT 4 (Band2).

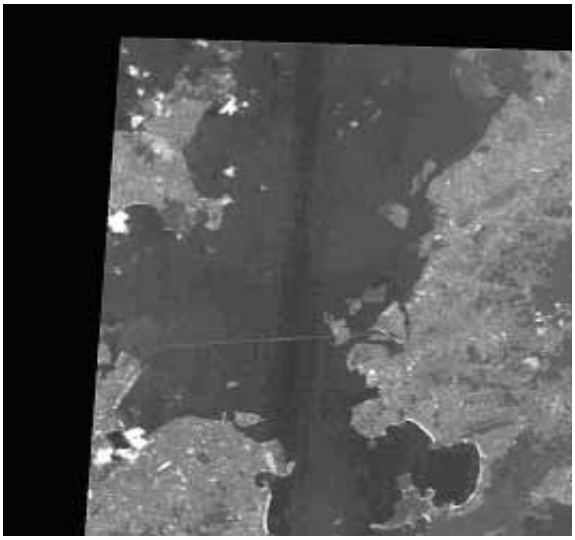

Fig.5.5 Registered CBERS Image (Rio-Niterói bridge).

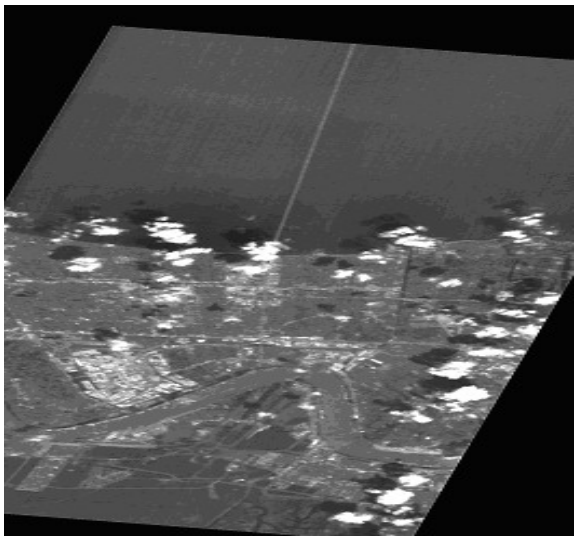

Fig.5.6 Registered CBERS image (Causeway bridge).

5.2 *PSF identification*

As in the previous sections, the point spread function is modeled as a 2D separable Gaussian function. In this experiment, the EIFOV estimation method is based on the degradation of SPOT-4 image so that its spatial resolution is similar to that of CBERS image (lower resolution). CBERS and SPOT-4 images must be well registered and the EIFOV value for each band of SPOT images must be known.

Let f be the original scene and let h_s be the SPOT-4 imaging system PSF. Then, the original SPOT-4 image is given by:

$$g_s = h_s * f \ .$$

Let h_d be the degradation filter PSF. Then SPOT-4 degraded image is given by:

$$g_d = h_d * g_s = h_d * (h_s * f) = (h_d * h_s) * f \ .$$

Finally, let h_c be CBERS CCD point spread function. Therefore, CBERS image is given by:

$$g_c = h_c * f \ .$$

To find CBERS PSF, h_c, one minimizes the "distance" between CBERS image g_c and SPOT-4 degraded image g_d by adjusting h_d. At the minimum, $g_d \approx g_c$ and $h_s * h_d$ is the estimation of h_c. Figure 5.7 shows the block diagram of the low-resolution image simulation process.

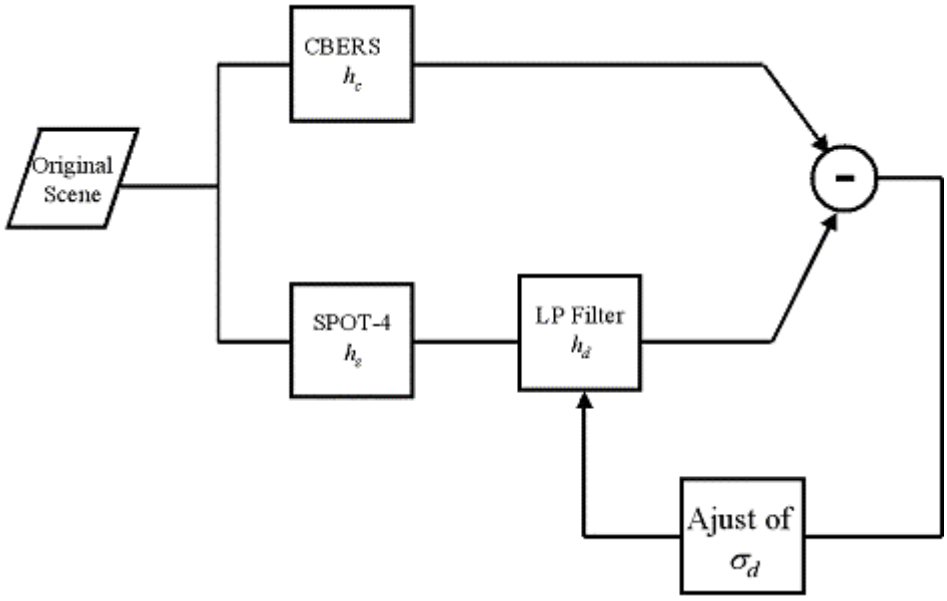

Fig.5.7 block diagram of the low-resolution image simulation process.

For the along- and across-track spatial resolution estimation, a three-step adjustment was performed. The first one consists of estimating a gain parameter to adjust the radiometry between CBERS and SPOT-4 images. The second step consists of finding an offset parameter that describes the residual registration error between both images. In the last step, the standard deviation parameter of the degradation filter is estimated, which is used to compute CBERS EIFOV values. In all steps the root-mean-square minimization is performed. Details about the method are presented below.

Let g_c be one column (one line) of CBERS Rio-Niterói (Causeway) bridge image and g_s be one column (one line) of SPOT-4 Rio-Niterói (Causeway) bridge image.

Let denote by $g_{\mu,\sigma}$ the degraded SPOT-4 image column (one line) that is:

$$g_{\mu,\sigma} = h_{\mu,\sigma} * g_s \quad ,$$

where

$$h_{\mu,\sigma}(x) = h_\sigma(x-\mu) \quad .$$

Step 1: Radiometric Adjust

In this step, the radiometric adjustment consists of estimating the gain parameter a that minimizes the root mean square difference between CBERS image column (line) and SPOT-4 image column (line). Hence, given an a priori value σ_0 we look for the parameter a that minimizes

$$\sum \left((ag_c + b) - g_{o,\sigma_0} \right)^2 ,$$

where $b = m - a.m_c$ (the initial value for a is s/s_c), m_c and s_c are the mean and standard deviation of g_c, and m and s are the mean and standard deviation of g_s.

Step 2: Offset Adjust

In this step, given the parameters a and b determined at step 1, one looks for μ that minimizes

$$\sum\left(\left(ag_c + b\right) - g_{\mu,\sigma_0}\right)^2.$$

Step 3: EIFOV Estimation

In this step, since the parameters *a*, *b* and μ have been determined, one looks for σ that minimizes

$$\sum\left(\left(ag_c + b\right) - g_{\mu,\sigma}\right)^2.$$

Therefore, given the σ parameter and the effective spatial resolution (EIFOVs) of SPOT-4 image, CBERS CCD effective spatial resolution (EIFOVc) is calculated by:

$$\mathrm{EIFOV}_c = 2.66\left(\left(\frac{\mathrm{EIFOV}_s}{2.66}\right)^2 + \sigma^2\right)^{1/2},$$

where EIFOVs is the along-track (across-track) spatial resolution of SPOT-4 system. The final EIFOV_c value is taken as the mean value of EIFOVc over all columns (or lines).

In the three steps described above, the parameters have been obtained by nonlinear programming (Himmelblau, 1972).

5.3 *Results*

Table 5.1 presents the EIFOV values for the SPOT-4 system used in this experiment. The estimated parameters of the CBERS-1 and CBERS-2 cameras are presented in the Tables 5.2 and 5.3, respectively. Fig 5.4 shows an example of curve fitting in along-track and across-track direction.

Table 5.1: SPOT-4 EIFOV

(Fonseca, 2004).

Bands	EIFOV (m) along-track direction	EIFOV (m) across-track direction
B2	28	27
B3	30	29
B4	31	34

Table 5.2: Estimated EIFOV for CBERS-1.

Bands	EIFOV (m) along-track direction	EIFOV (m) across-track direction
B2	34	65
B3	37	64
B4	54	77

Table 5.3 Estimated EIFOV for CBERS-2.

Bands	EIFOV (m) along-track direction	EIFOV (m) across-track direction
B2	34	59
B3	39	59
B4	36	63

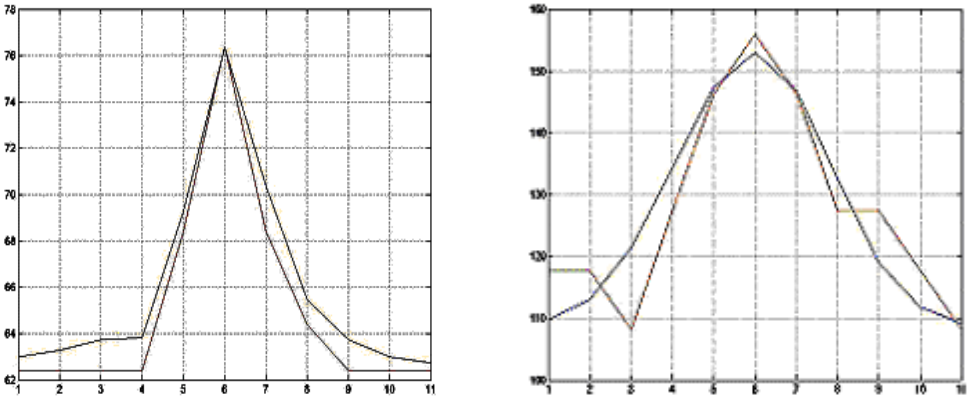

Fig 5.4 Fitting: (a) along-track and (b) across-track direction.

The results are similar to those obtained by simulated and natural target methods. The mean EIFOV values (CBERS-2) obtained from the three experiments are shown in Table 5.4. The results are similar to those obtained by Sun et al. (2004), which are presented in the Table 5.5; the EIFOV values, in the across-track direction, are somewhat bigger than the ones obtained by Sun et al. (2004).

Table 5.4: Mean EIFOV for CBERS-2 obtained in this work.

Bands	EIFOV (m) along-track direction	EIFOV (m) across-track direction
B2	35	59
B3	43	58
B4	37	63

Table 5.5: Mean EIFOV for CBERS-2 obtained by (J. Jun Sun, 2004).

Bands	EIFOV (m) along-track direction	EIFOV (m) across-track direction
B2	34	53
B3	40	53
B4	39	51

6. Conclusion

In this work, three methodologies to estimate the effective spatial resolution of CBERS-1 and CBERS-2 CCD cameras have been presented. Broadly speaking, the estimation process consisted of finding the best fit between the image and the simulated target image. The targets used in the experiments were bridges and an artificial target simulated in the Gob Desert (China). In all experiments the results showed that the spatial resolution in across-track direction does not conform to the specification for all bands of CBERS-1 and CBERS-2. This problem can be explained by the vibration effect provoked when both IRMSS and CCD sensors work simultaneously or also by the electronic coupling between adjacent detectors. As expected, band 4 of CBERS-1, in along-track direction, is not in accord with the camera specification. On the other hand, band 4 (CBERS-2) presented better spatial resolution than that of the specification and band 3 (CBERS-2) presented worse spatial resolution than the one specified in along-track direction.
The methodologies developed in this work have been implemented in the CBERS Image Processing System as part of a module that is responsible for evaluating the quality of CBERS images.

References

BANON, G. J. F. **Formal introduction to digital image processing**. São José dos Campos: INPE, 2000. (INPE-7682-PUD/097). <http://iris.sid.inpe.br:1912/rep-/dpi.inpe.br/banon/1999/06.21.09.31>.

BANON, G. J. F. Simulação de imagens de baixa resolução (portuguese). **Controle & Automação**, v. 2, n. 3, p. 180-192, Mar/Apr 1990.

BANON, G. J. F.; FONSECA, L. M. G. **CBERS simulation from SPOT and its restoration** (in portuguese). São José dos Campos, SP, Brazil: Instituto Nacional de Pesquisas Espaciais - INPE, 1998. <http://iris.sid.inpe.br:1912/>.

BANON, G. J. F.; SANTOS, A. C. **Digital filter design for sensor simulation: application to the Brazilian Remote Sensing Satellite**. Sao Jose dos campos: INPE, 1993. 62 p. (INPE-5523- RPQ/665). Posted in the UR*Lib* digital library: <dpi.inpe.br/banon/1995/12.14.18.12>.

BENSEBAA, K.; BANON, G. J. F.; FONSECA, L. M. G. On-orbit spatial resolution estimation of CBERS-1 CCD imaging system. In: International Conference on Image and Graphics (ICIG 2004), 3., 18-20 dec. 2004, Hong Kong, China. **Proceedings**… Los Alamitos, CA: IEEE Computer Society Press, 2004. v. 2 p. 576-579.

BENSEBAA, K.; BANON, G. J. F.; FONSECA, L. M. G. On-orbit Spatial Resolution Estimation of CBERS-1 CCD Imaging System from bridge images. In: Congress International Society for Photogrammetry and Remote Sensing, 20., 12-23 July 2004, Istanbul, Turkey**. Proceedings**… Istambul: International Archives of Photogrammetry, Remote Sensing and Spatial Information Sciences, 2004, v. 35, part B1, p. 36-41.

BENSEBAA, K.; BANON, G. J. F.; FONSECA, L. M. G. On-orbit spatial resolution estimation of CBERS-1 CCD imaging system using higher resolution images. In: Simpósio Brasileiro de Sensoriamento Remoto (SBSR), 12., 2005, Goiânia, p. 827-834. CD-ROM. ISBN 85-17-00018-8. <http://marte.dpi.inpe.br/col/ltid.inpe.br/sbsr/2005/02.12.16.31/doc/>.

Choi, T. and D. Helder. On-Orbit Modulation Transfer Function (MTF) Measurement. **Remote Sensing of Environment**, v. 88, p. 42.45, 2003.

FEDOROV, D.; FONSECA, L. M. G.; MANJUNATH, B. S; KENNEY, C. Automatic Registration and Mosaicking System for Remotely Sensed Imagery. International Symposium on Remote Sensing, International Society for Optical Engineering (SPIE), 22-27 September 2002, Crete, Greece.

FEDOROV, D.; FONSECA, L. M. G.; MANJUNATH, B. S; KENNEY, C. Automatic Registration and Mosaicking System. http://regima.dpi.inpe.br. Acess in: 2006, April.

FONSECA, L. M. G. **SPOT-4 Spatial Resolution Estimation**. Personal communication.

FONSECA, L. M. G.; PONZONI, F; CARTAXO, R. **Radiometric quality assessment of CBERS-2.** São Jose dos Campos: INPE 2004. APPL-06-2004.

FONSECA, L. M. G.; ESCADA, J; PONZONI, F. **A Preliminary assessment of geometric and radiometric quality for CBERS-1 CCD instrument.** São Jose dos Campos: INPE 2002. APPL-02-2002.

FONSECA, L. M. G.; MASCARENHAS, N. D. D. Determination of the Landsat-5 TM Modulation Transfer Function (portuguese). Congresso Nacional de Matemática Aplicada e Computacional, 10., 21-26 set. 1987, Gramado, BR. São José dos Campos: INPE, 1987. p. 297-302. INPE-4213-PRE/1094.

HIMMELBLAU, D. M. **Applied nonlinear programming**. New York: McGraw- Hill, 1972.

KREYSZIG, E. **Advanced engineering mathematics.** New York: John Wiley and Sons, 1993.

LEGER, D.; VIALLEFONT-ROBINET, F.; MEYGRET, A. In-flight refocusing and MTF assessment of SPOT5 HRG and HRS cameras. In: SPIE International Symposium on optical and Technology, 9., 23-27 set. 2002, Agia Pelagia, Crête, Greece. **Proceedings**… Agia Pelagia: SPIE, 2002.

LUXEN, M.; FORSTNER, W. Characterizing image quality: Blind estimation of the point spread function from a single image. In: ISPRS Commission III Symposium (Photogrammetric Computer Vision), 9-13 Setember 2002, Graz, Austria. **Proceedings**… Graz: PCV02, 2002, v. XXXIV, part 3A, p. 205–210.

MARKHAM, B.L. The Landsat sensor's spatial response. **IEEE Transactions on Geoscience and Remote Sensing**, v. 23, n. 6, p. 864-875, nov. 1985.

NELSON, N.R.; BARRY, P.S. Measurement of hyperion MTF from on-orbit scenes. In: The International Symposium on Optical Science and Technology (SPIE), 46., July 29 - August 3, 2001, San Diego, CA. **Proceedings**… San Diego: SPIE, 2001, v. 4480 p. 236-241.

SLATER, P.N. **Remote sensing optics and optical system**. London: Addison-Wesley, 1980.

STOREY, J. C. Landsat 7 on-orbit modulation transfer function estimation. In: Sensors, Systems, and Next Generation Satellites 5., 17-20 sep. 2001, Toulouse, France. **Proceedings**… Bellingham, WA, USA: SPIE, 2001, p. 50-61.